02481

LA-UR-10-~~01605~~

Approved for public release; distribution is unlimited.

Title:	Measurements of Residual Stress in Fracture Mechanics Coupons
Author(s):	Michael R. Hill, U.C. Davis John E. VanDalen, Hill Engineering, LLC Michael B. Prime, W-13
Intended for:	SEM Annual Conference & Exposition on Experimental and Applied Mechanics Indianapolis, Indiana USA June 7 - 9, 2010

Los Alamos
NATIONAL LABORATORY
EST. 1943

Form 836 (7/06)

Measurements of Residual Stress in Fracture Mechanics Coupons

Michael R. Hill[1], John E. VanDalen[2] and Michael B. Prime[3]
[1]Mechanical and Aerospace Engineering Department,
University of California, One Shields Avenue,
Davis, CA 95616 USA, mrhill@ucdavis.edu
[2]Hill Engineering, LLC, McClellan, CA USA
[3]Los Alamos National Laboratory, Los Alamos, NM USA

ABSTRACT

This paper describes measurements of residual stress in coupons used for fracture mechanics testing. The primary objective of the measurements is to quantify the distribution of residual stress acting to open (and/or close) the crack across the crack plane. The slitting method and the contour method are two destructive residual stress measurement methods particularly capable of addressing that objective, and these were applied to measure residual stress in a set of identically prepared compact tension (C(T)) coupons. Comparison of the results of the two measurement methods provides some useful observations. Results from fracture mechanics tests of residual stress bearing coupons and fracture analysis, based on linear superposition of applied and residual stresses, show consistent behavior of coupons having various levels of residual stress.

INTRODUCTION

Fracture mechanics testing typically relies on test coupons being free from residual stress, though limited guidance is provided to ensure that coupons are stress free. For materials that cannot be tested in coupons free from residual stress, it may be that measured residual stress can be used to obtain a test outcome (i.e., fracture mechanics properties) independent of residual stresses.

The superposition of stress intensity factors provides a basis for residual stress corrections that might be applied for properties determined under generally linearly elastic, small scale yielding conditions, such as low-energy fracture (brittle or ductile in nature) or fatigue crack growth in metallic materials. Superposition of stress intensity factors (SIFs) under monotonic or cyclic loading can be expressed simply as

$$K_{Tot} = K_{App} + K_{RS} \tag{1}$$

where K_{App} is the SIF from applied loads, K_{RS} is the SIF from residual stress, and K_{Tot} is the total SIF. Testing standards (e.g., ASTM E399, E647, and so forth) provide expressions for K_{App} while K_{RS} would be determined using newly established standard procedures.

The objective of this work is to provide example measurements of the opening-direction residual stress on the crack plane, and the residual stress intensity factor, in fracture coupons containing various levels of residual stress. This paper is a follow-up to recently reported work that contains details of fracture tests on the same set of coupons [1].

METHODS

Material and geometry

Aluminum alloy 7075-T6 was selected for this test program due to its prevalent use in a variety of applications. This alloy exhibits low-energy ductile fracture with a rising *R*-curve. The material was received as clad plate 4.8 mm thick. Handbook [2] mechanical properties of 7075-T6 are listed in Table 1.

Compact tension, C(T), coupons were used in this study, as described in several of the ASTM fracture toughness testing standards (e.g., ASTM E 561-98 – "Standard Practice for *R*-Curve Determination"). The C(T)

coupon is well suited for this work because of its accepted use in fracture toughness testing, simple geometry, and one-dimensional crack, characterized by the crack length *a*. Coupon geometry had thickness *B* of 3.81 mm and a characteristic width dimension *W* of 50.8 mm (Fig. 1). Coupons were cut such that crack growth occurred in the L-T orientation. To obtain the 3.8 mm coupon thickness from the stock material, material was machined in equal amounts from each side so that the coupons lay in the T/2 plane and the original clad layer was removed. A starter notch with integral knife edges for crack mouth opening displacement (CMOD) was cut into each coupon using a wire electric discharge machine (EDM). The EDM notch was 0.3 mm wide and had various lengths, as described below.

S_u (MPa)	S_y (MPa)	E (GPa)	ν	K_{Ic} (MPa m$^{0.5}$)
552	490	71	0.33	29.0

Table 1 – Mechanical properties of 7075-T6 plate [2]

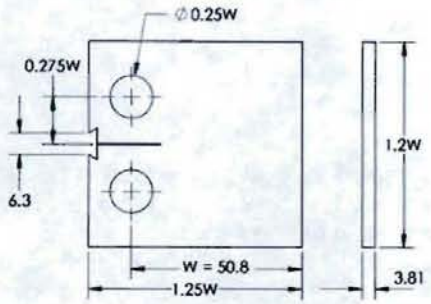

Fig. 1 – 7075-T6 C(T) Coupon (dimensions in mm)

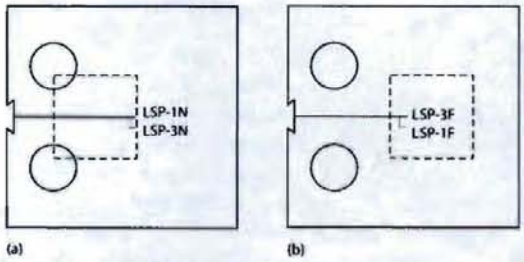

Fig. 2 – Location of LSP regions (square regions enclosed by dashed line, having side length of 22.9 mm) (a) near the front face (12.7 mm from the front face) and (b) far from the front face (12.7 mm from the back face) (also shown are initial crack lengths used for fracture tests of the coupon sets)

Residual stress treatment

Laser shock peening (LSP) was used to produce residual stress bearing coupons. In thin geometries, like the C(T) coupons used here, LSP can generate through-thickness compressive residual stress in the treated area. The LSP process uses laser-induced shocks to drive plastic deformation into the surface of a part [3,4]. For this work, LSP was applied using industrial facilities at Metal Improvement Company (Livermore, CA). LSP parameters were chosen to achieve high levels of residual stress in the C(T) coupons. Earlier work in high strength aluminum alloys found that deep residual stress was induced in 19 mm thick coupons using an LSP parameter set of 4 GW/cm^2 irradiance per pulse, 18ns pulse duration, and 3 layers of treatment (denoted 4-18-3) [5,6]. It was further found that 4-18-3 provided significant high-cycle fatigue life improvements in 19 mm thick bend bars.

For the present work, LSP was used to obtain two *amounts* of residual stress effect and either *positive* or *negative* residual stress effect on fracture toughness. To obtain sets of coupons with different amounts of residual stress, LSP was applied using a single layer, at 4-18-1, or using three layers, at 4-18-3, where three-layer LSP induces a greater amount of residual stress. To obtain sets of coupons with either positive or negative residual stress effects on fracture, LSP was applied in two different areas, each a square with side length of 22.9 mm and located either *near to* or *far from* the front face of the C(T) coupon (Fig. 2). Applying LSP near the front face results in compressive residual stress on the crack faces, providing a negative contribution to fracture (i.e., a negative residual stress intensity factor), while applying LSP far from the from the front face results in tensile residual stress on the crack faces, providing a positive contribution to fracture. In total, five coupon conditions were used in this study: as-machined (AM); one-layer LSP applied near the front face (LSP-1N); three-layer LSP applied near the front face (LSP-3N); one-layer LSP applied far from the front face (LSP-1F); and, three-layer LSP applied far from the front face (LSP-3F). LSP coupons were treated on both sides, alternating sides between each layer application until each side was treated with the desired number of layers.

Residual stress and K_{RS} measurements

Two-dimensional residual stress distributions were measured on the prospective crack plane of AM and LSP-3N coupon blanks using the contour method [7,8]. Measurements were made on C(T) blanks that had holes, but did not have initial notches. Wire EDM was used to cut the coupons in half and expose the crack plane. After cutting, an area-scanning profilometer was used to measure the resulting out-of-plane deformation of the cut surface, on both halves of the coupon. The measured deformations of the two halves were averaged and smoothed to remove effects of cut path wandering, shear stress, and surface roughness. The negative of the averaged and smoothed deformations were applied as displacement boundary conditions in a three-dimensional, linear elastic finite element model of one-half of the coupon. The stress resulting from the elastic finite element calculation provided the experimental estimate of residual stress in the coupon.

Thickness average residual stresses were measured in all coupon conditions using the slitting method. A strain gage with an active grid length of 0.8 mm was applied to the center of the back face of the coupon (opposite the crack mouth). Wire EDM was used to incrementally extend a slit through the coupon, with strain recorded after each increment of slit depth. Residual stress as a function of position across the coupon was determined from strain versus slit depth data using the approach recently described by Schajer and Prime [9] and adapted to the geometry of the C(T) coupon.

Measured residual stresses from slitting and contour are compared to one another to determine the degree of consistency among the methods employed. The comparison is made on thickness-average residual stress as a function of position across the crack plane, with the two-dimensional stresses from the contour measurements averaged at a set of positions across the crack plane.

The slitting method was also used to determine the residual intensity factor as a function of crack length, $K_{RS}(a)$, following Schindler's method for a thin rectangular plate [10]. $K_{RS}(a)$ was computed from the influence function $Z(a)$ provided in [10], the plane stress modulus of elasticity $E' = E$ (given in Table 1), and the derivative of strain with respect to slit depth

$$K_{RS}(a) = \frac{E'}{Z(a)} \frac{d\varepsilon(a)}{da}. \qquad (2)$$

The influence function $Z(a)$ of [10] does not account for the holes present in the C(T) coupon, which was assumed to be of negligible effect. In addition, care was taken to account for the different definitions of crack size used by ASTM (measured from the load-line) and Schindler (measured from the front edge), which can cause error (or misinterpretation of results, as in [11]). The derivative of strain with respect to crack length was computed using a moving five-point quadratic polynomial, with slope evaluated numerically at the middle point.

Residual stress intensity factors were computed from measured residual stress using a Green's function for the C(T) coupon recently published by Newman, et al [12] and numerical integration, paying careful attention to the singularity of the Green's function [13]. Residual stress intensity factors computed from measured residual stresses are compared against those determined from Eqn. (2).

Fracture toughness tests were performed according to ASTM E 561-98 to determine the K-R crack growth resistance curve for each of the five coupon conditions. Replicate tests were run for each condition. Details can be found in our earlier work [1]. The K-R results are presented in terms of applied loading alone, and in terms of total residual stress intensity factor (Eqn. (1)). In addition, initiation toughness was determined in the coupons using data collected during K-R testing, but using the data reduction procedures of ASTM E 399 to determine K_Q.

RESULTS

Residual stress fields on the crack plane determined using the contour method are illustrated in Fig. 3 for two AM and one LSP-3N coupons. Residual stress in the AM coupons have peak values around ±20 MPa and have a similar through thickness distribution at all points across the coupon width, which is consistent with residual stress from plate rolling. The LSP coupon has a maximum compressive residual stress of -290 MPa that occurs on the surface near the middle of the coupon, and a maximum tensile stress of 350 MPa that occurs at the front face of the coupon. In the peened region (from x = 12.7 to x = 35.6 mm, where x is measured from the front face of the coupon), residual stress is compressive at the surfaces and grows more positive monotonically with position toward the coupon mid-thickness. Outside the peened region, residual stress is nearly uniform through thickness but varies with position across the width. The residual stress distribution features inside the LSP region are consistent with double sided peening and outside the LSP region are consistent with plate bending and axial stresses that arise in the coupon to achieve residual stress equilibrium (zero net force and moment across the contour plane).

Slitting residual stress measurements show that the location of the peened area significantly affects the stress distribution across the coupon (Fig. 4). LSP near the front face of the coupon (LSP-1N and LSP-3N) produces tensile stresses at the front face that give way to compression 12 to 16 mm from the front face. LSP far from the front face (LSP-1F and LSP-3F) creates tensile stresses at the front face and over a region extending 26 to 30 mm from the front face. For the same peened area, the shape of the stress distributions for one-layer and three-layer LSP are quite similar, with 3-layer LSP coupons having about twice as much residual stress.

Thickness average residual stress for the LSP-3N and one of the AM coupons is plotted in Fig. 5. AM coupons have a thickness-average stress of nearly 0 MPa at all points across the coupon, which is consistent with plate rolling. Thickness-average stress in the LSP-3N coupon has maximum tension at the front face (240 MPa) and maximum compression (-150 MPa) near the middle of the LSP area (x = 28 mm). The slitting residual stress measurement has a higher gradient near the right edge of the peened area (x = 36 mm) than shown for the contour residual stress, but the two measurements are in good agreement (Fig. 5). The difference may be due to surface fitting in the contour data reduction, which softens (spatial) stress gradients.

Estimates of K_{RS} were determined from strain versus depth data using two different procedures, and these are compared in Fig. 6. The first procedure used Eqn. (2), above, and results are shown as symbols in Fig. 6. The second procedure used the residual stress from slitting, reported in Fig. 4, the Green's function of Newman, et al [12], and numerical integration, and the resulting K_{RS} estimates are shown as lines in Fig. 6. There is good agreement between the two calculation procedures. For condition LSP-3N, K_{RS} was also computed using the Green's function and contour thickness-average residual stresses (Fig. 5). The estimates of K_{RS} show good agreement, except for the negative peak in K_{RS}, which appears softened when using the contour stresses and may be the result of surface smoothing (Fig. 7).

At initial crack lengths useful for fracture tests ($0.35W$ = 18 mm $\le a_o \le 0.55W$ = 28 mm), K_{RS} estimates show that $K_{RS}(a)$ is either negative or positive, depending on the location of the LSP area (Fig. 6). At these crack lengths, the far-from-front-face LSP coupons (LSP-1F, LSP-3F) have positive K_{RS} and the near-front-face LSP coupons (LSP-1N, LSP-3N) have negative K_{RS}. K_{RS} for the three-layer LSP coupons (LSP-3F, LSP-3N) are roughly double those for the corresponding one-layer LSP coupons (LSP-1F, LSP-1N). For LSP-3F, the positive K_{RS} reaches 35.9 MPa $m^{0.5}$, which is quite large, exceeding the material plane strain fracture toughness of 29.0 MPa $m^{0.5}$ (Table 1). The magnitude of the most positive K_{RS} in coupons LSP-1F and LSP-3F (17.7 and 35.9 MPa $m^{0.5}$) is nearly twice the magnitude of the most negative K_{RS} in coupons LSP-1N and LSP-3N (-10.5 and -16.8 MPa $m^{0.5}$).

Based on the slitting results (Fig. 6), target initial crack lengths were selected for K-R fracture tests. The target crack lengths chosen for each condition are shown (to scale) with the LSP area in Fig. 2. Compression-compression precracking was performed for the LSP-1F and LSP-3F coupons due to the high magnitude, positive K_{RS} (for further precracking and other details of fracture testing, refer to our earlier work [1]).

Results of fracture testing showed significant and expected effects from LSP-induced residual stress. R-curves in terms of K_{app} are shown for all coupons in Fig. 8. Results for the two AM coupons exhibit typical elastic-plastic blunting behavior until about 30 MPa $m^{0.5}$, after which monotonically increasing (nearly linear) crack growth resistance is obtained. Compared with the AM results at a given crack length, the LSP-1N and LSP-3N coupons exhibit greater toughness (in terms of K_{app}) and the LSP-1F and LSP3F coupons exhibit reduced toughness, with the 3-layer coupons having a larger effect in both cases. Comparing results for the two coupons within each coupon subset shows the data to be repeatable. Residual stress corrected R-curves were prepared using Eqn. (1) and using values of K_{RS} determined from Eqn. (2). The corrected R-curves for the different coupon subsets are similar (Fig. 9). The LSP-1N and LSP-3N results exhibit significantly greater elastic-plastic blunting than for the AM coupons, which is consistent with the higher level of applied loading at which they initiate crack extension. After blunting, the R-curves of all coupon subsets are in good agreement, though the LSP-3F coupons exhibit a significantly shallower R-curve.

Values of initiation toughness are very significantly affected by residual stress in terms of applied load (K_Q) but are nearly invariant in terms of total stress ($K_{Q,Tot}$) (Fig. 10). The mean K_Q for AM coupons was 33.1 MPa $m^{0.5}$, a value slightly greater than K_{Ic} (Table 1), which is expected given the limited coupon thickness. Mean K_Q values for residual stress bearing coupons ranged from 9.69 MPa $m^{0.5}$ for LSP-3F coupons to 51.6 MPa $m^{0.5}$ for LSP-3N coupons. Mean $K_{Q,Tot}$ values ranged from 32.1 MPa $m^{0.5}$ (LSP-3F) to 37.4 MPa $m^{0.5}$ (LSP-1N), with the latter value being somewhat of an outlier.

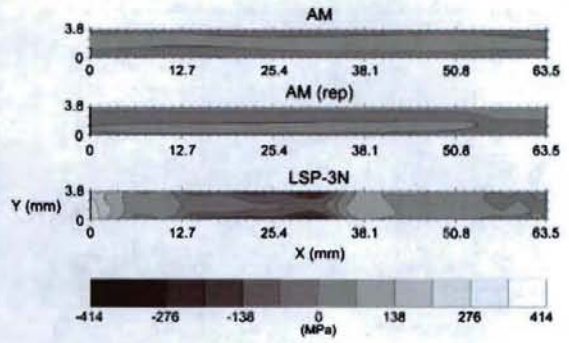

Fig. 3 – Contour measurement results illustrating the residual stress distribution on the plane of the crack for AM and LSP-3N coupons ("rep" indicates a replicate (identical) coupon)

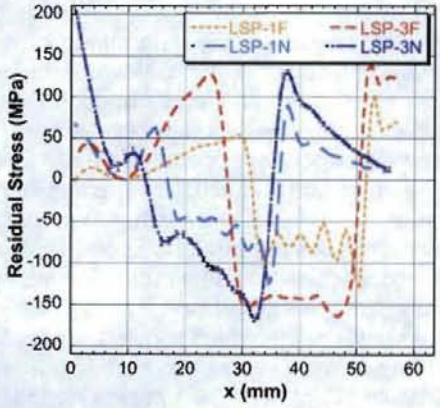

Fig. 4 – Slitting residual stress measurement results (AM condition not measured); one-sigma error bars are plotted for LSP-3N, other conditions exhibit similar levels of uncertainty

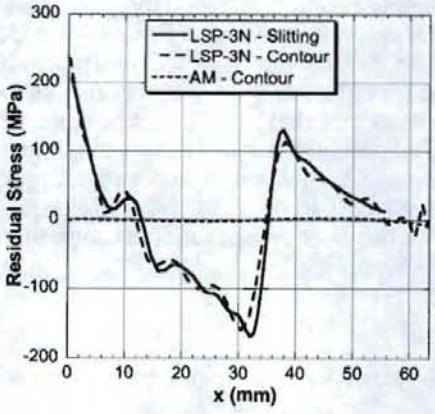

Fig. 5 – Slitting residual stress for LSP-3N plotted with contour through thickness average for LSP-3N and AM conditions

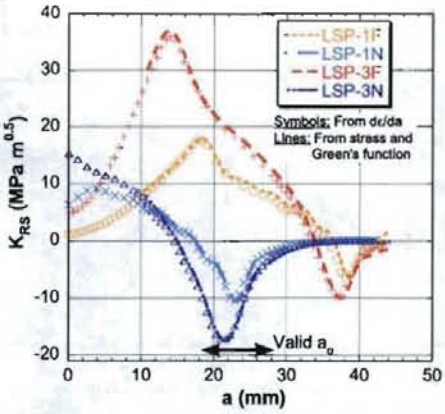

Fig. 6 – Comparison of K_{RS} determined from slitting strain data: symbols are determined from derivative of strain data (Eqn. (2)); lines result from integrating residual stress of Fig. 4 with the Green's function for the C(T) coupon published by Newman, et al. [12]

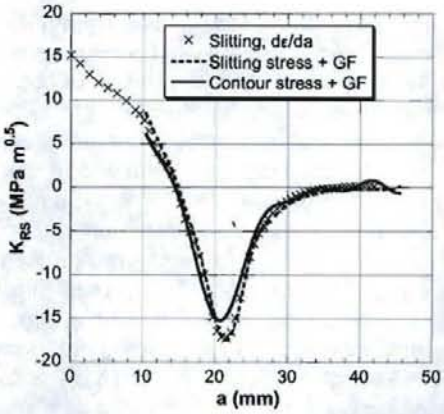

Fig. 7 – K_{RS} for LSP-3N condition computed from derivative of strain data (Eqn. (2)), and measured residual stress from slitting and contour thickness-average stress

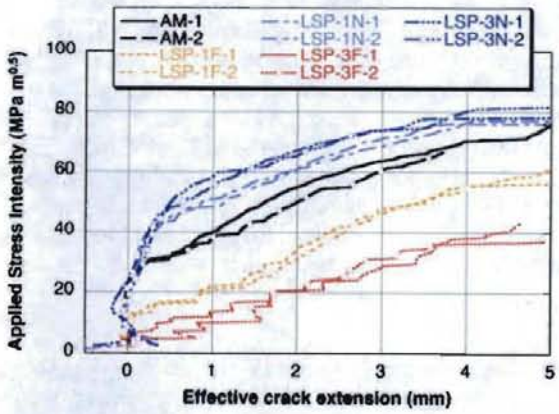

Fig. 8 – R-curve resulting from applied stress intensity factor

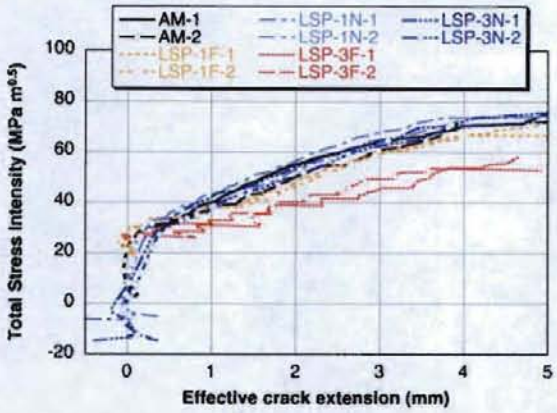

Fig. 9 – R-curve resulting from superposition of applied and residual stress intensity factors; $K_{RS}(a)$ from symbols in Fig. 6

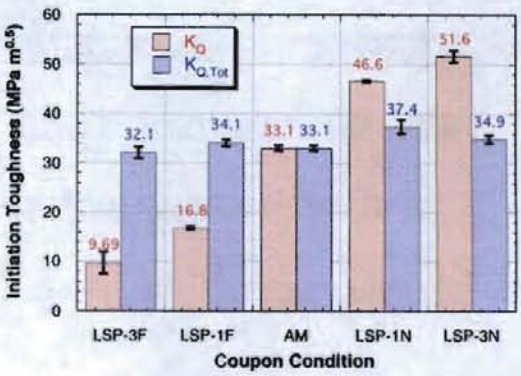

Fig. 10 – Comparison of K_Q and $K_{Q,Tot}$ for the five coupon conditions (bars and values provide mean, error bars indicate range from two coupons) ; $K_{RS}(a)$ from symbols in Fig. 6

SUMMARY

The present work describes measurements of residual stress in fracture coupons, the determination of residual stress intensity factors (as a function of crack length) from measured stress and more directly using Schindler's method [10], and correlation of observed fracture behavior in high-strength aluminum coupons. The results demonstrate consistent fracture property measurements in residual stress bearing coupons, where residual stress was taken into account; however, the consistency here was dependent on specific methodological choices. First, the material employed is one that exhibits low-energy fracture, and as such, has fracture behavior that is influenced directly (in fact, linearly) by K_{RS}. It remains to be determined whether consistent toughness data could be obtained in residual stress bearing coupons of a significantly more ductile material. Second, fracture toughness and K_{RS} measurements were performed on coupons prepared identically. A test program employing coupons with greater variability (e.g., hand-forgings or welded materials) likely would provide less-consistent results. Third, the coupon geometry had a large width-to-thickness ratio ($W/B \approx 13$), which allowed significant residual stress influence while avoiding complications arising from variations of K_{RS} along the crack front and the potential for non-straight crack fronts (e.g., as for welded joints [14]). While slitting was the best method for the present coupons, a significantly smaller width-to-thickness ratio might require accounting for through-thickness stress variation (e.g., measured by the contour method) and its affect on K_{RS} along the crack front. Follow-on work would need to determine the range of material, coupon geometry, and residual stress fields for which consistent fracture toughness properties can be obtained.

Method selection is an important step when making material property measurements, and the inclusion of residual stress in fracture property testing would require additional standardization activity. Here, the slitting method directly provided $K_{RS}(a)$ from Eqn. (2), which was readily combined with test data. The values of $K_{RS}(a)$ from Eqn. (2) were in very good agreement with those determined from residual stress and Green's function. Slitting was straightforward to implement and the method offers good repeatability (see replicate results for the present coupons reported in [1], as well as repeatability of residual stress reported in [15]). Active standardization of the slitting method, within ASTM Task Group E28.13.02, supports its potential use in fracture toughness testing standards. The good agreement for initiation toughness $K_{Q,Tot}$ and R-curve behavior shown here among coupons containing significantly different distributions of residual stress suggest a course of further work to extend standard fracture toughness tests so that they include residual stress effects for an appropriate range of material, coupon geometry, and residual stress fields.

REFERENCES

[1] VanDalen, J. E. and Hill, M. R., "Evaluation of residual stress corrections to fracture toughness values," Journal of ASTM International, **5**(8), Paper ID JAI101713.

[2] United States Department of Transportation – Federal Aviation Administration, 2003, Metallic Materials Properties Development and Standardization, Report DOT/FAA/AR-MMPDS-01.

[3] Fabbro, R., Peyre, P., Berthe, L., and Scherpereel, X., 1998, "Physics and applications of laser-shock processing," Journal of Laser Applications, **10**, pp. 265-279.

[4] Montross, C.S., Wei, T., Ye, L., Clark, G., and Mai, Y.-W., 2002, "Laser shock processing and its effects on microstructure and properties of metal alloys: a review," International Journal of Fatigue, **24**, pp. 1021-1036.
[5] Pistochini, T., 2003, "Fatigue Life Optimization in Laser Peened 7050-T7451 and 300M Steel," M.S. Thesis, Department of Mechanical and Aeronautical Engineering, University of California, Davis.
[6] Luong, H., 2006, "Fatigue life extension and the effects of laser peening on 7050-T7451 aluminum, 7085-T651 aluminum, and Ti-6Al-4V titanium alloy," M.S. Thesis, Department of Mechanical and Aeronautical Engineering, University of California, Davis.
[7] Prime, M.B., 2001, "Cross-sectional mapping of residual stresses by measuring the surface contour after a cut," Journal of Engineering Materials and Technology, **123**, pp. 162-168.
[8] Prime, M.B., Sebring, R.J., Edwards, J.M., Hughes, D.J., and Webster, P.J., 2004, "Laser surface-contouring and spline data-smoothing for residual-stress measurement," Experimental Mechanics, **44**, pp. 176-184.
[9] Schajer, G.S., and Prime, M.B., 2006, "Use of Inverse Solutions for Residual Stress Measurements," Journal of Engineering Materials and Technology, **128**, pp. 375-382.
[10] Schindler, H.J. and P. Bertschinger, 1997, "Some steps towards automation of the crack compliance method to measure residual stress distributions," in Proceedings of the 5th International Conference on Residual Stress, Linköping.
[11] Ghidini, T., Donne, C. D., 2007, "Fatigue crack propagation assessment based on residual stresses obtained through cut-compliance technique," Fatigue and Fracture of Engineering Materials and Structures, **30**, pp. 214-222.
[12] Newman, J.C., Yamada, Y., James, M.A., 2010, "Stress-intensity-factor equations for compact specimen subjected to concentrated forces," Engineering Fracture Mechanics, **77**, pp 1025-1029.
[13] Wu, X.-R. and Carlsson, A.J., 1991, Weight function and stress intensity factor solutions, Pergamon Press, pp. 37-38.
[14] Towers, O.L., Dawes, M.G., 1985, "Welding Institute research on the fatigue precracking of fracture toughness specimens," in *Elastic-Plastic Fracture Test Methods: The User's Experience, ASTM STP 856*, American Society for Testing and Materials, Philadelphia, PA, p. 23-46.
[15] Lee, M.J., Hill, M.R., 2007, "Intralaboratory repeatability of residual stress determined by the slitting method," *Experimental Mechanics*, **47**, pp. 745-752.